Experimental and theoretical study of used GFRP I-profile composite columns

Mohammed Abdel-Rahman M. Khalil, Ata El-Kariem Shoeib Soliman, Alaa Gamal Sheriff, Mohammed M. Salem
Faculty of Engineering, Helwan University, Egypt.
mamkhalil@m-eng.helwan.edu.eg, atta_alsayed@m-eng.helwan.edu.eg, agbsherif@gmail.com, Mohamedsalem@m-eng.helwan.edu.eg

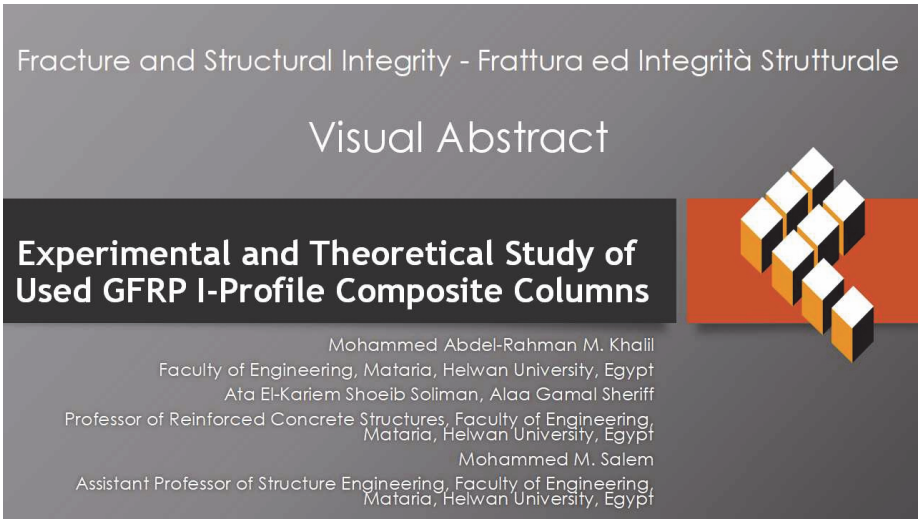

OPEN ACCESS

Citation: Khalil, M., Soliman, A., Sheriff, A., Salem, M., Experimental and theoretical study of used GFRP I-profile composite columns, Fracture and Structural Integrity, 72 (2025) 263-279.

Received: 19.01.2025
Accepted: 23.03.2025
Published: 26.03.2025
Issue: 04.2025

KEYWORDS. GFRP I-Section, Composite columns, Reinforced concrete columns, Fire, Experimental results, theoretical study and Finite element Analysis.

INTRODUCTION

The study of Glass Fiber Reinforced Polymer (GFRP) composite columns under axial load is increasingly important in civil engineering due to the growing adoption of composite materials in construction. GFRP offers advantages such as a high strength-to-weight ratio, corrosion resistance, and durability. However, its limitations include poor fire resistance, lower ductility, and potential long-term deflection concerns. When combined with concrete, GFRP-reinforced columns can enhance load-bearing capacity and ductility compared to conventional reinforced concrete (RC) columns. The structural behavior of GFRP-concrete composite columns depends on factors such as the type and ratio of GFRP, the bond between GFRP and concrete, and the level of confinement provided. Understanding these interactions is crucial for designing safe, efficient structures. Further research is needed to refine design guidelines and optimize material usage, leading to cost-effective solutions for structural applications.
Several studies have investigated the axial load performance of GFRP-reinforced composite columns. Muhammad et al. [1] examined GFRP I-section and C-section composite columns under axial and eccentric loads. Their results showed that GFRP I-section-reinforced columns achieved higher ultimate loads but exhibited lower ductility compared to steel-reinforced columns. Jing et al. [2] studied concrete-filled square GFRP tubular columns under axial

compression and found that reinforcement cages significantly improved load capacity and ductility. Muhammad et al. [3] further investigated GFRP tube-reinforced concrete columns, concluding that GFRP tubes enhance both ductility and strength. Ishaqian and Keramti [4] confirmed that pultruded GFRP I-shapes effectively improve concrete column performance. However, Zureick and Scott [5] identified global buckling as the primary failure mechanism in slender GFRP-reinforced columns. Hashem [6] conducted analytical and experimental research on short and long GFRP composite columns, while Lei [7] investigated slender GFRP square hollow columns under axial and eccentric loads and revealed that the compression performance of GFRP columns was significantly affected by the eccentricity and the moment capacity of bolted sleeve joint. Srinath T [8] conducted an experimental and numerical investigation on the bonding and buckling behavior of GFRP circular column under axial compression, and results showed more performance than similar conventional. Srinath et al. [8] studied the bonding and buckling behavior of GFRP circular columns under axial compression. Hiba et al. [9] found that composite columns with encased GFRP I-sections outperformed traditional columns under various loading conditions. Aydin [10] evaluated GFRP profile strength at different temperatures, reporting that tensile and compressive strengths decreased by 28% and 75%, respectively, at 100°C compared to ambient conditions. At 200°C, GFRP lost approximately 50% of its tensile strength and all its compressive strength due to the degradation and softening of the polymer matrix within the GFRP components at high temperatures, resulting in reduced load carrying capacity. In addition, exposure to fire causes thermal expansion mismatches between the GFRP and concrete layers, inducing cracking and delamination effects, which further reduce structural performance.

GFRP profiles exhibit high sensitivity to elevated temperatures but remain stable under lower temperature conditions. Therefore, fire resistance must be carefully considered when using GFRP in high-temperature environments. This study investigates the behavior of composite columns reinforced with GFRP I-section subjected to 500°C for 90 minutes. Experimental, theoretical, and numerical analyses, including finite element modeling, are conducted to assess axial load performance. A practical design guideline for optimizing GFRP-reinforced composite columns is proposed to enhance structural efficiency and cost-effectiveness. All specimens are tested under axial loading, with load-strain behavior and failure modes analyzed to provide insights into the structural performance of GFRP-concrete composite columns.

EXPERIMENTAL PROGRAM

The experimental study of this research is based on testing the behavior of GFRP-concrete composite columns under axial load. The column samples are shown schematically in Fig. 1, and they consist of the following:

Test parameters and specimen details

Two main parameters are considered: the effect of GFRP I-section on the behavior of RC composite columns and the effect of fire. The concrete dimensions and reinforcement details of the tested columns are given in Tab. 1 and Fig. 1. A total of four specimens were fabricated and tested in this experimental study.

All tested columns had an overall height of 1540 mm and a cross section of 160 mm x160 mm. They were reinforced with longitudinal four steel bars of 10 mm diameter and steel transverse stirrups of 8 mm diameter at 100 mm spacing. The GFRP I-section had a total height of 100 mm, a flange width of 80 mm and a web and flange thickness of 5.5 mm positioned centrally within the RC composite columns. All of the specimens had the same concrete cover of 15 mm.

Specimens Code	Dim. (mm) H	b	Steel Longitudinal	Stirrups	Fire	GFRP I -sec	Notes
RCC	1540	160	4R10	R8@100/mm	----	----	Reference for (RCCGI-C & RCC-F)
RCCGI-C	1540	160	4R10	R8@100/mm	----	In center	As comparison for (RCC) The Reference for (RCCGI-C-F)
RCC-F	1540	160	4R10	R8@100/mm	Fire	----	As comparison for (RCC)
RCCGI-C-F	1540	160	4R10	R8@100/mm	Fire	In center	As comparison for (RCCGI-C)

Note that:
RCC: The tested conventional reinforced concrete column,
GI : The GRPR I-section
C : Center position
F : Fire

Table 1: Designations of tested columns.

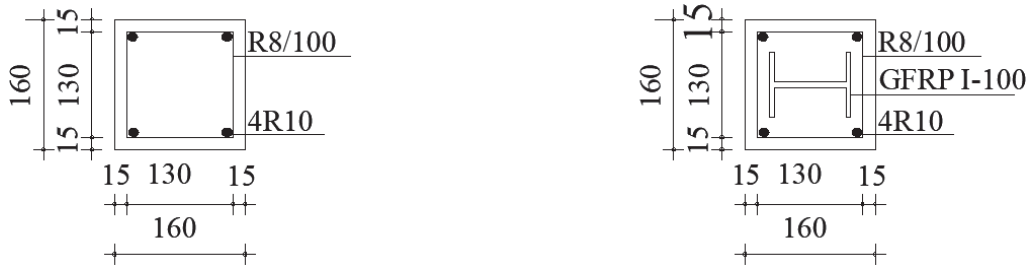

a) RCC and RCC-F b) RCCGI-C and RCCGI-C-F

Figure 1: Specimens details of tested column (mm).

Material properties

The concrete used was cement (Sina Cement Company) (450 kg/m³), natural siliceous sand, crushed dolomite coarse aggregate of maximum size 12.5 mm and super plasticizer's (Addicrete BVS type G) **2**% from the weight of the cement. The target mean strength was **45** MPa. The mix had a water-cement (w/c) ratio of 0.37, cement content of 500 kg/m³, fine aggregate content of 628 kg/m³, coarse aggregate content of 1144 kg/m³, and super- plasticizer content of 10 kg/m³. Nine standard cubes with dimensions 150 mm x 150 mm x 150 mm were cast to perform concrete quality control. The cubes were immersed in water until the day of testing. The **35**-day strength achieved was the average compressive strength of **46** MPa at the test day.

The yield strength and ultimate strength of smooth steel bars were 316 MPa and 431 MPa for 8 mm stirrups bars, and 470 MPa and 636 MPa for 10 mm respectively. The results of steel bars are summarized in Tab. 2.

No. of samples	Length (mm)	Diameter. (mm) Nominal	Actual	Tensile strength (Mpa) f_y	f_u	Elongation (%)	Specification elongation
5	500	8	8.15	304	415	61	≥20%
5	500	10	10.12	470	636	32	≥16%

Table 2: Results of steel bars properties.

The mechanical properties of the used GFRP I-section are shown in Tab. 3 according to manufacturer's date [11] obtained from standard tests, the tensile strength of GFRP I-section was 336 MPa, and tensile modulus of elasticity 35300 MPa.

No.	Item	Data
1	Specific gravity	1.85 g/cm³
2	Tensile strength	336 MPa
3	Tensile modulus	35300 MPa
4	Flexural strength	334 MPa
5	Flexural modulus	73000 MPa
6	Compressive strength	327 MPa
7	Impact strength	2385 J/M
8	Hardness	52 HRC
9	Water-absorption rate	1.39 %

Table 3: GFRP I-section properties.

Test setup and instrumentation

The test setup of axial compressive loading for the tested columns is presented in Fig. 2. The test columns were simply supported by steel plates at two ends. The column specimens were tested using the test frame as shown in Fig. 2 was fixed to the strong solid floor of the RC laboratory at the Faculty of Engineering of Helwan University. The supporting setup consisted of a horizontal frame made of four steel I-beams, supported by four vertical steel I-beam legs installed on the strong solid floor. The tested columns were rested on the frame. Loading was achieved by using a 1250 kN capacity cell, which transferred the axial load to a steel plate with high rigidity at the top of the columns, set up as shown in Fig. 2.

The load was measured by a 1250 kN capacity load cell, which was connected to a digital display unit. The horizontal sway and vertical displacement at the points shown in Fig. 3a were measured using two linear variable differential transducers (LVDTs) and two dial gauges (DGs) with an accuracy of 0.01mm.

The (LVDTs) and (DGs) were placed on the side and top surface of the columns as shown in Fig. 3b. Four electrical strain gauges were used to measure the strain in the steel bars and GFRP I-section at the maximum tensile point of

the steel bars and GFRP I-section as shown in Fig. 4. This measurement location was maintained for all tested columns.

Figure 2: Axial load that transfer from load cell to columns.

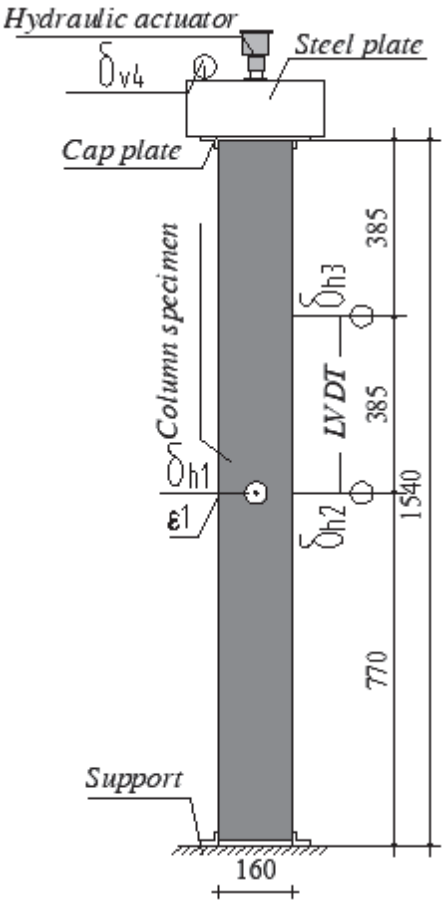

a)Position

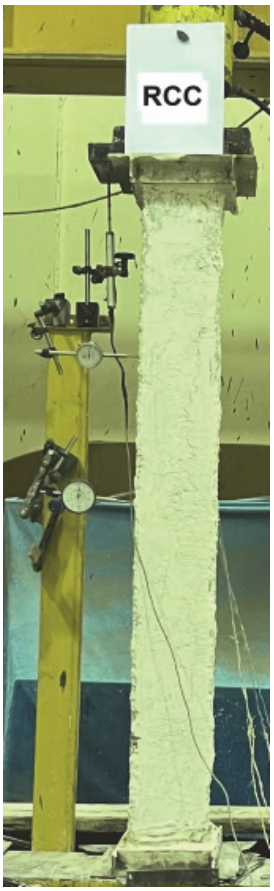

b) Arrangement

Figure 3: Dial gauges and LVDTs.

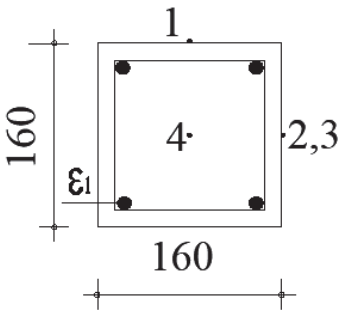

a) Conventional column

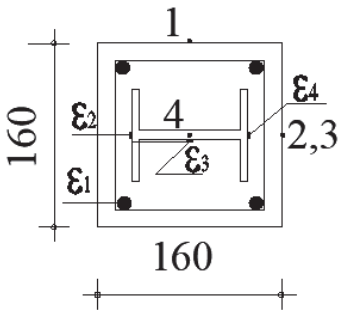

b) Composite columns

Figure 4: Test setup LVDT, DG and strain gauges of columns (mm).

Procedure for firing

The RC column specimens were placed in a circular steel frame with side holes through which the fire was ignited. The specimens were exposed to a fire at 500°C for 90-minutes as shown in Fig. 5. After exposure, the RC columns were allowed to cool at room temperature for more than 4 hours before being loaded to failure. A wired digital reader with thermal sensor was used to stabilize the temperature at 500°C for 90-minutes duration.

a) During the fire b) After the fire

Figure 5: Specimens during the fire.

RESULTS AND DISCUSSION

Failure modes of columns

The failure modes of the columns of all tested specimens are clearly shown in Fig. 6. All the tested specimens exhibited concrete compression failure under axial load and splitting of the reinforcing steel bars, which occurred after the concrete, reached its ultimate stress value. In addition, collapse occurred in GFRP I-section flanges of the tested RC composite column, as shown in Fig. 6b. The concrete failed at the mid height of the column due to deterioration in the polymers when exposed to fire. This was caused by the flammability of the organic resin matrix used in the GFRP I-section components, leading to significant weakening, as observed in the fire-exposed RC composite column in Fig. 6d.

a) RCC

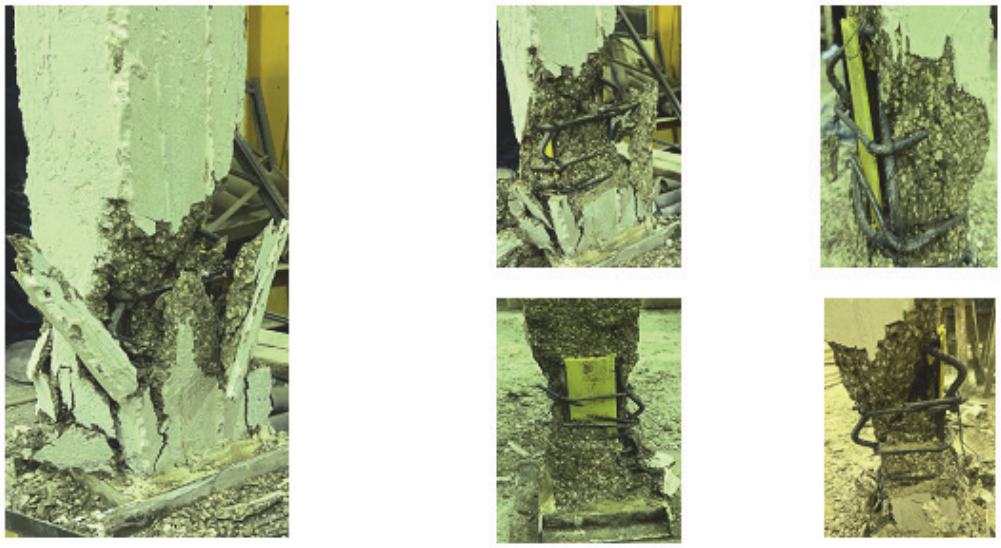

b) RCCGI-C

c) RCC-F

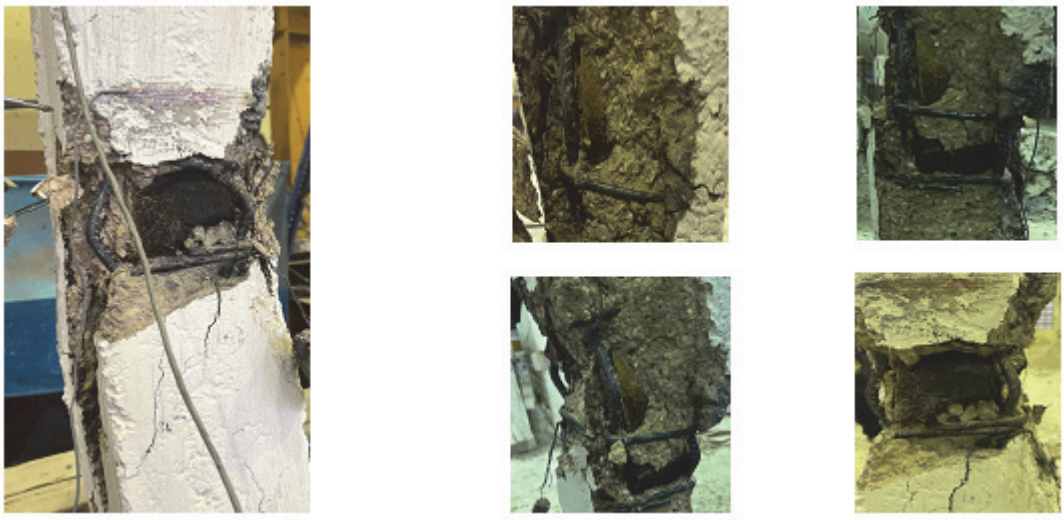

d) RCCGI-C-F

Figure 6: Failure modes of tested columns.

Cracking of the columns started the applied loads reached more than 83% of the maximum load for the reinforced concrete columns without fire and 94% of the maximum load for the columns exposed to fire, respectively.

Cracking and maximum load

The cracking and maximum loads are summarized in Tab. 2. The results show that the composite RC columns achieved 117% of the axial load bearing capacity of the conventional RC columns. While, the composite circular encased GFRP I-section columns achieved 9.7% higher maximum load than the conventional RC columns under a compression load of 25 mm eccentricity [9]. The conventional RC columns exposed to fire achieved 86% of the capacity compared to the RC columns without fire. Meanwhile, the RC composite columns exposed to fire achieved 61% of the capacity compared to RC composite columns without fire due to the flammability of the organic resin matrix used in the GFRP compounds.

The results shown in Fig. 7 indicate that the maximum bearing capacity was achieved in RC composite column. The maximum reduction in column bearing capacity was observed in the GFRP I-profile RC composite column exposed to fire.

Specimens Code	Cracking Load (kN)	Maximum Load (kN)	P_{cr}/P_u	P_u/P_{uCtrl}	Notes
RCC	996.24	1052.90	94.62	1.00	Reference for (RCCGI-C & RCC-F)
RCCGI-C	1165.46	1234.30	94.42	1.17	As comparison for (RCC) The Reference for (RCCGI-C-F)
RCC-F	766.30	900.71	85.08	0.86	As comparison for (RCC)
RCCGI-C-F	621.73	746.99	83.23	0.61	As comparison for (RCCGI-C)

Table 4: The experimental results.

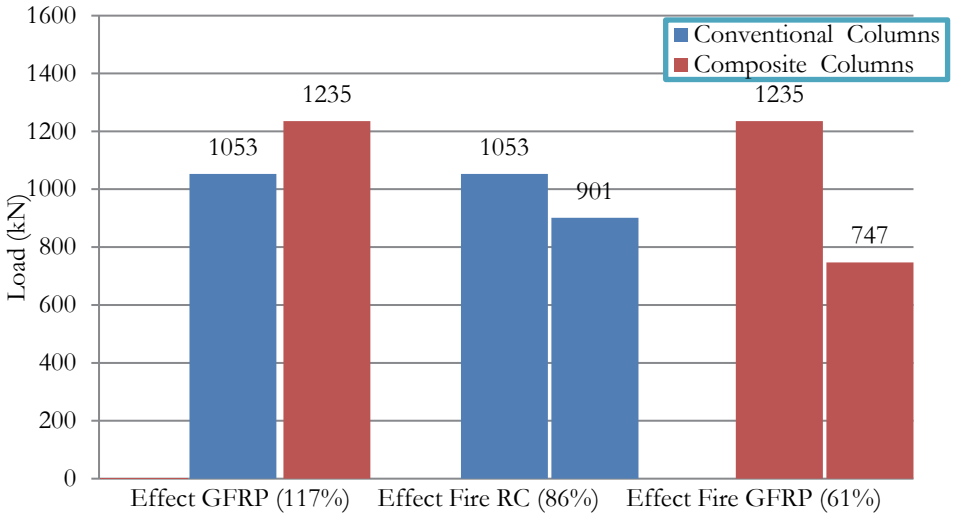

Figure 7: The maximum load and comparison between of tested columns.

Comparing the maximum loads of the tested columns, it can be noted that the maximum load of the RC composite columns without fire was higher than that of the conventional RC columns. In the RC composite columns, the maximum load increased to 117% compared to conventional RC columns.

Load–displacement curves

The load–vertical displacement relationships for the tested conventional columns and RC composite columns are shown in Fig. 8. The displacement values were measured at the top height point of the RC columns.

The axial stiffness of the tested columns represents their resistance of the columns to deflection or deformation under axial load. Stiffness is defined as the ratio of ultimate load to ultimate deflection [12]. The axial stiffness of conventional RC columns without fire was higher than that of RC composite columns, with values of 131.61 kN/mm and 85.94 kN/mm, respectively. The axial stiffness of the tested columns without fire was also higher than that of RC columns exposed to fire. The axial stiffness of conventional RC columns was 131.61 kN/mm without fire and 80.27 kN/mm with fire. For the RC composite columns, the axial stiffness was 85.94 kN/mm without fire and 59.52 kN/mm with fire. The reduction in stiffness for the fire-exposed specimens was due to increased deformation.

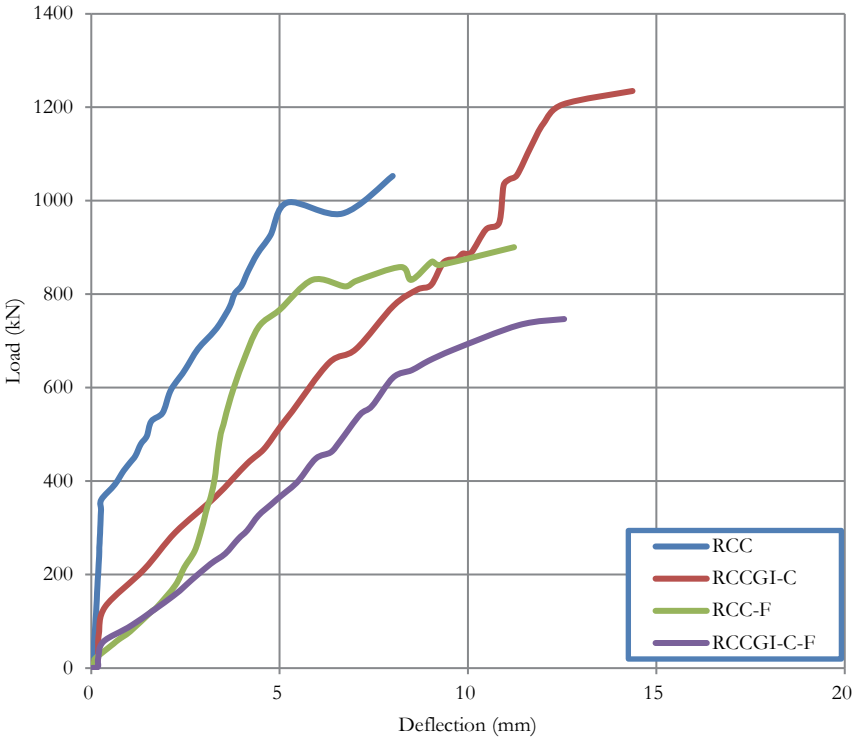

Figure 8: Load vertical displacement curves of tested columns.

The comparison between the conventional RC columns and the RC composite columns without fire shows that the RC composite columns are more ductile than the conventional RC columns.

Stress strain curves

The measured stress-strain curves of the tested RC composite column without fire are shown in Fig. 9. The axial strain in steel bars and GFRP I-section exhibited similar behavior at the same load level, recording low strains values of the tested column without fire. In contrast, the transverse strain in the GFRP I-section was significantly lower compared to the axial strain. In general, the maximum strain in the steel bars and GFRP I-section did not reach half of the yielding strain of the steel bars**.** Fig. 9 for the RC composite column shows strain compatibility in deflection, indicating that both the internal steel and GFRP materials within the columns experienced similar strains and deformations when subjected to axial load.

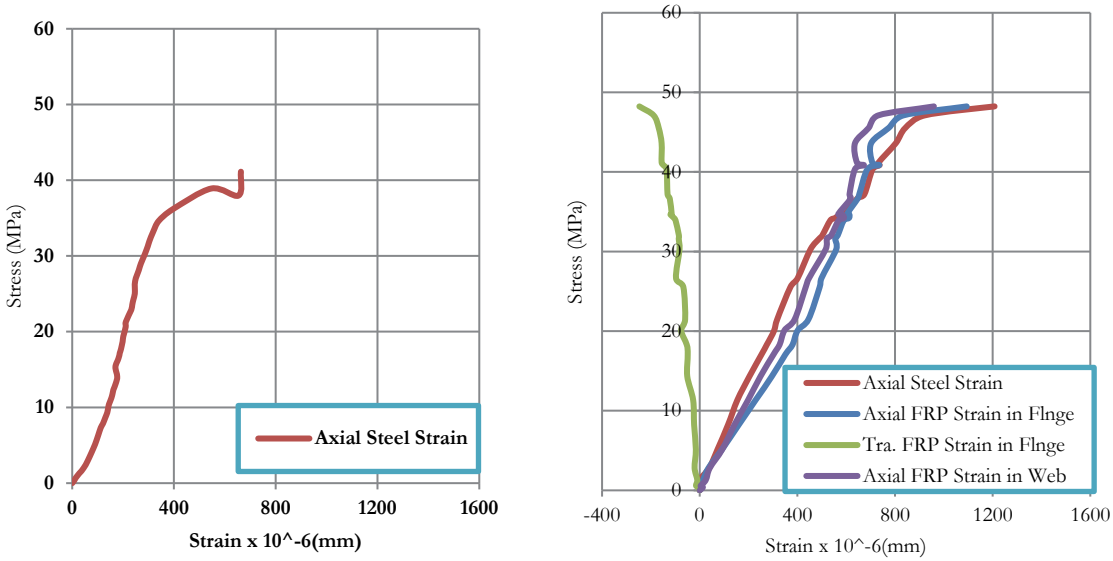

a) Conventional column b) Composite columns

Figure 9: The stress-strain curves of conventional and composite columns without firing.

THEORETICAL ANALYSIS

The ability of common structural analysis tools to predict the performance of the tested RC composite columns was investigated to provide practicing engineers with information on their reliability according to the different codes.

The ultimate strength of the conventional RC columns was calculated at the point of failure, the theoretical ultimate strength or nominal strength of a short axially loaded column can be determined accurately by the using Egyptian Code of Practice (ECP-203) [13] and British Standard BS 8110-97 [14]. The theoretical maximum load can be calculated by considering the contributions of both the concrete and reinforcement in bearing the axial load, as follows;

$$P_n = 0.67 f_{cu}\left(A_g - A_{st}\right) + f_y A_{st} \tag{1}$$

According to ACI 318-11 [15], the theoretical maximum load can be calculated by considering the contribution of both the concrete and the reinforcement in carrying the axial load;

$$P_n = 0.85 f_c^{'}\left(A_g - A_{st}\right) + f_y A_{st}\,. \tag{2}$$

The maximum nominal axial load on a column is calculated using the following equation according to Eurocode [16];

$$P_n = \eta f_c^{'}\left(A_g - A_{st}\right) + f_y A_{st}\,. \tag{3}$$

where;

$$\eta = 1 \qquad \text{for } f'c \le 50 \text{ MPa} \tag{4}$$

$$\eta = 1.0 - \left(f_c^{'} - 50\right)/200 \qquad \text{for } 50 < f'c \le 90 \text{ MPa} \tag{5}$$

$$f_s = \varepsilon_c E_s \tag{6}$$

$$\varepsilon_c = 2\% \qquad \text{for } f'c < 50 \text{ MPa} \tag{7}$$

$$\varepsilon_c(\%) = 2.0 + 0.085\left(f_c^{'} - 50\right)^{0.53} \qquad \text{for } f'c \ge 50 \text{ MPa} \tag{8}$$

The maximum nominal axial load on the column is calculated using the following equation according to CSA A23.3-0[17];

$$P_n = a_1 \varphi_c f_c^{'}\left(A_g - A_{st}\right) + \varphi_s f_y A_{st} \tag{9}$$

$$a_1 = 0.85 - 0.0015 f_c^{'} \qquad \text{but not less than } 0.67 \tag{10}$$

By comparing the experimental results with the values calculated using the theoretical equation of the different codes, it w found that the experimental and theoretical results calculated by the Egyptian Code of Practice (ECP-203) [13], British Standard BS 8110-97 [14], and ACI 318-11 [15] converge very closely for the axial load. This indicates the auracy and reliability of the findings as the theoretical results align well with the experimental observations, showing no significant differences in axial loads as presented in Tab. 3. Therefore, the following proposed equation is recommended to calculate the axial load of RC composite columns based on the Egyptian Code of Practice, and other Standard codes as following;

E-203 & BS $\quad P_n = 0.67 f_{cu}\left(A_g - A_{st} - A_f\right) + f_y A_{st} + 0.65 f_f A_f\,.$ (11)

A $$P_n = 0.85 f_c^{'} \left(A_g - A_{st} - A_f \right) + f_y A_{st} + 0.65 f_f A_f \quad (12)$$

Eurocode $$P_n = \eta f_c^{'} \left(A_g - A_{st} - A_f \right) + f_y A_{st} + 0.65 f_f A_f \quad (13)$$

C $$P_n = a_1 \varphi_c f_c^{'} \left(A_g - A_{st} - A_f \right) + \varphi_s f_y A_{st} + 0.65 f_f A_f \quad (14)$$

The reinforced concrete columns exposed to fire at 500 degrees, according to Eurocode 1991-1-2, section 3 [16], ruire the application of reduction factors $k_{c,\theta}$, and $k_{y,\theta}$, to to the compressive strength of concrete and the yield strength of steel, respectively. For conventional reinforced concrete columns, these reduction factors are 0.74 for concrete and 0.78 for steel. These reduction factors can also be applied to composite columns. However, the resistance of GFRP should be neglected due to the melting of the organic resin matrix used in GFRP compounds at high temperatures.

Specimens	Maximum load (kN)					$P_{exp.}$ / $P_{theo.}$			
Code	$P_{exp.}$	$P_{ECP\& BS}$	$P_{ACI.}$	$P_{EUR.}$	$P_{CSA.}$	ECP& BS	ACI	EUR	CSA
RCC	1052.90	1043.04	1055.55	1129.69	1005.50	1.01	1.00	0.93	1.05
RCCGI-C	1234.30	1232.74	1243.74	1299.72	1199.75	1.00	0.99	0.95	1.03
RCC-F	900.71	-------	-------	841.12	-------	-------	-------	1.07	------
RCCGI-C-F	746.99	--------	--------	751.54	--------	--------	--------	0.99	------

Table 5: Comparison between experimental and theoretical results of composite columns.

The theoretical calculations and the accuracy of the proposed equation based on different codes were able to accurately predict the load-carrying capacity of composite columns under vertical load.

NUMERICAL ANALYSIS

The non-linear finite element analysis method, as well as, the finite element analysis by using ANSYS (R19) was considered. The columns exhibited non-linear behavior primarily due to the inherent nonlinear material, elastic-plastic behavior of the steel reinforcement bars and the linear-pseudo plastic and brittle behavior of the concrete. This analysis method is currently regarded as the state-of-the art for analyzing reinforced concrete structures. However, the use of this sophisticated tool is complicated by the need to select several control parameters, which are typically chosen based on prior experience in finite element results with experimental data from similar structures. In addition to replicating the behavior of the tested columns without fire exposure, the non-linear analyses were conducted to study the effects of the concrete compressive strength, steel yield strength, reinforcement ratio, and of the GFRP ratio in the composite columns. The analysis was performed using the finite element package ANSYS [18].

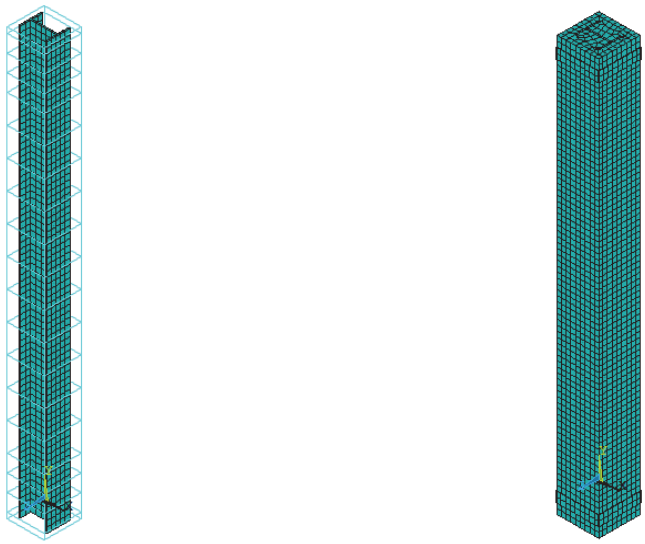

a) Link elements for steel bars and GFRP I-section b) Solid elements for concrete & steel plates

Figure 10: The model of the column used in the nonlinear analysis.

Modeling

The solid element SOLID65 was used to model the concrete, while the 3D spar Link180 element was used to model the steel bars. The solid element SOLID185 was utilized to model the GFRP I-section and steel plates at the column supports. The model of the verification column is shown in Fig. 10.

Material properties

Eqn. (1), proposed by MacGregor [19], is used to represent the uniaxial compressive stress-strain relationship for concrete.

$$f = \frac{E_c \varepsilon}{1 + \left(\frac{\varepsilon}{\varepsilon_o}\right)^2} \tag{15}$$

This equation has been used to plot the multi-linear isotropic stress-strain curve for concrete from 0.3fc' to the ultimate compressive strength, *0.3fc'*.the Elastic modulus is defined as 0.3fc', and calculated in the linear region. The elastic-plastic uniaxial stress-strain model was used to model reinforcing steel. Additionally, the modulus of elasticity and the tensile strength of concrete were calculated using the same specifications. The stress-strain curves of steel bars were presented according to the ECP 203 Code of Practice [13]. The GFRP was assumed to be linear, elastic and orthotropic material, with material properties provided by the manufacturer input into the model. The elastic-plastic uniaxial stress-strain model from the ECP 203 Code of Practice [13] was also used to model the steel.

Validation of the numerical nonlinear model

For the validation of the ANSYS model for the RC composite columns, the parameters controlling the details of the concrete material model (SOLID65), such as tensile stiffening and shear retention across cracks of the reinforced concrete, were determined empirically by identifying the values that provided the best fit between the calculated stress-strain curve of the RC composite column and the experimental curve. The best-fit numerical curve and the experimental curve are shown in Fig. 11. In general, the numerical curve closely matches the experimental one. However, it is relatively less stiff than the experimental curve.

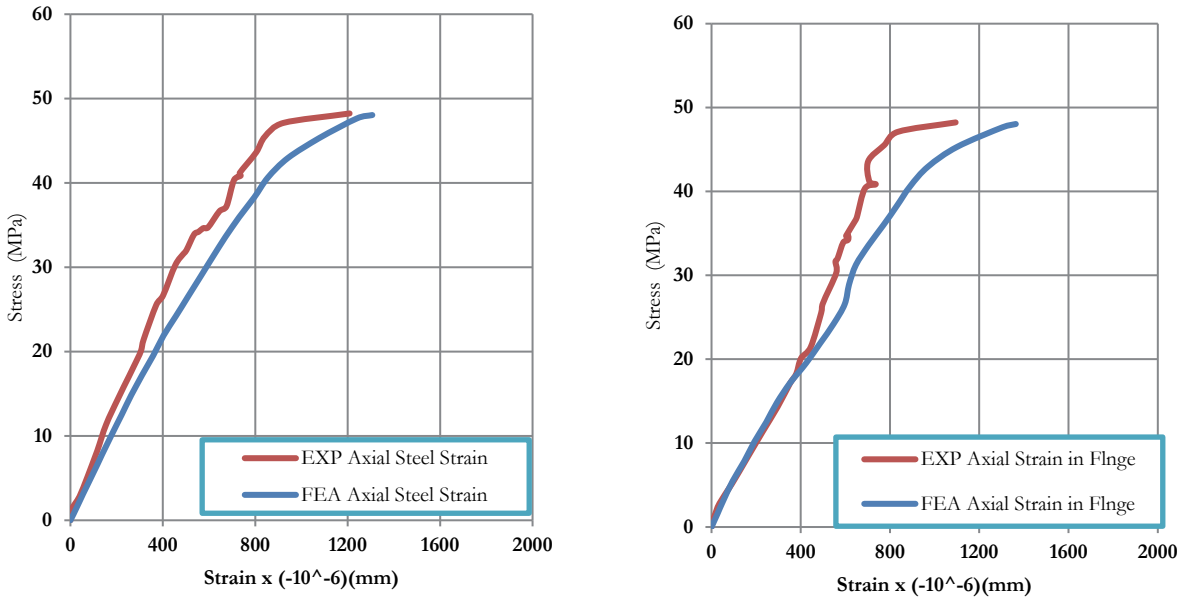

a) Axial strain of steel bars b) Axial strain of GFRP I-section

Figure 11: The experimental and numerical stress-strain curves of verification column.

Parametric study

After the verification of the finite element model, four parameters were further investigated for both the conventional RC columns and the RC composite columns:

(i) Effect of the compressive strength of concrete,
(ii) Effect of the yield strength of steel,

(iii) Effect of reinforcement ratio, and
(iv) Effect the of GFRP I-section ratio in the RC composite columns.

Through this investigation, the proposed equation for calculating the axial load of RC composite columns can be verified.

Effect of concrete compressive strength

To investigate the influence of normal and high compressive strength concrete on the bearing capacity of columns, nine analyses were performed for concrete strengths ranging from 20 MPa to 100 MPa for both conventional RC columns and RC composite columns.

The theoretical calculated maximum axial loads, based on the Egyptian Code of Practice (ECP-203) [13] and British Standard BS 8110-97 [14], along with the numerically calculated maximum axial loads from finite element analysis, are presented in Tab. 4 and Fig. 12. It is noted that the calculated maximum axial loads closely agree with the numerical values with deviations not exceeding 2% for conventional RC columns and 4% for RC composite columns, except when the compressive strength of concrete is equal to 20 MPa. In this case, the maximum axial loads calculated by finite element analysis shows an 8% increase compared to the maximum axial load calculated using the proposed equation for RC composite columns.

No.	Concrete compressive strength (F_{cu}) (MPa)	Conventional columns			Composite columns		
		P_{Equ} (kN)	P_{FEM} (kN)	P_{FEM}/P_{Equ}	P_{PEqu} (kN)	P_{FEM} (kN)	P_{FEM}/P_{PEqu}
CSC1	20	543.52	542.00	1.00	816.25	881.00	1.08
CSC2	30	712.88	701.00	0.98	976.44	1020.00	1.04
CSC3	40	882.24	880.00	1.00	1136.63	1160.00	1.02
CSC4	50	1051.61	1050.00	1.00	1296.81	1340.00	1.03
CSC5	60	1220.97	1212.00	0.99	1457.00	1470.00	1.01
CSC6	70	1390.33	1382.00	0.99	1617.19	1580.00	0.98
CSC7	80	1559.69	1530.00	0.98	1777.38	1760.00	0.99
CSC8	90	1729.06	1721.00	1.00	1937.56	1970.00	1.02
CSC9	100	1898.42	1921.00	1.01	2097.75	2180.00	1.04

Table 6: Effect of concrete compressive strength on theoretical and numerical maximum axial load.

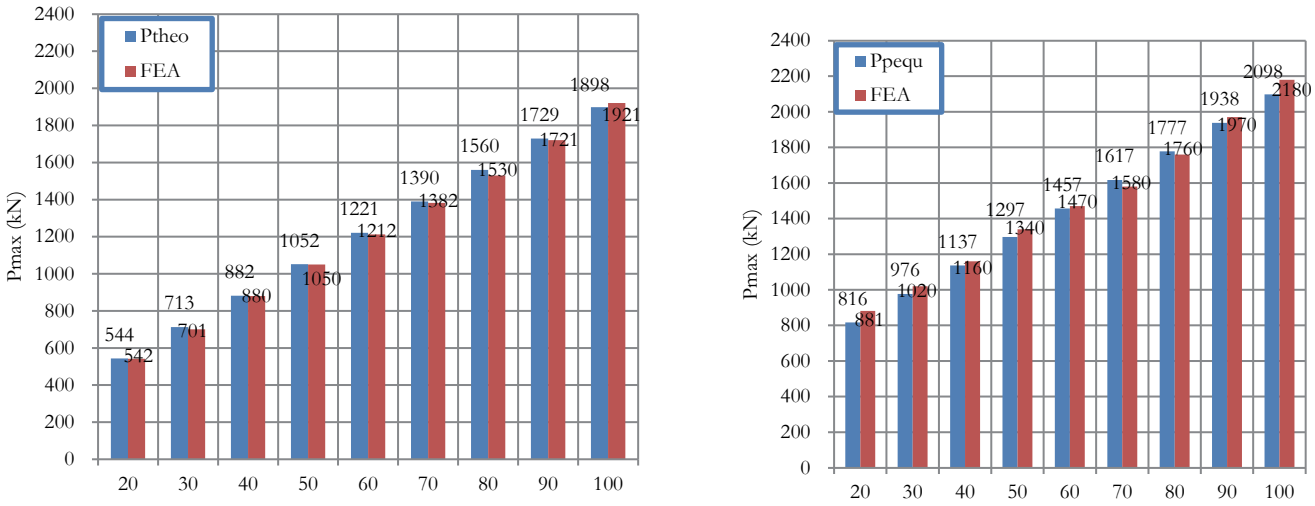

a) Conventional column b) Composite columns

Figure 12: Effect of concrete compressive strength on theoretical and numerical maximum axial load.

Fig. 13 shows the relationship between the compressive strength of concrete and the axial load for conventional RC columns and RC composite columns. It can be seen that the axial load increases linearly with the increase in the compressive strength of concrete.

Effect of yield strength of steel

The yield strength of steel does not significantly affect the axial load capacity of conventional RC columns, as shown in Tab. 5, and does not apply to RC composite columns. All stresses in the longitudinal reinforcement were monitored in theoretical specimens through finite element analysis based on the previous parameters. It is noted that the

maximum stress in steel bars is less than 300 MPa for concrete compressive strengths up to 50 MPa. For high-strength concrete (100 MPa), the stress in the steel bars reaches 525.33 MPa. Therefore, Eurocode [16] assumes that the stress in the longitudinal steel is equal to the young's modulus of steel multiplied by the strain in concrete when it reaches its maximum strength.

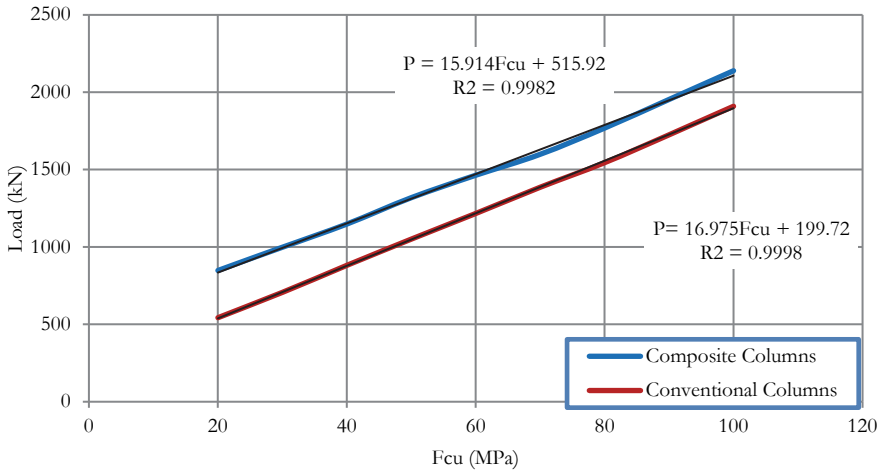

Figure 13: Relationship between concrete compressive strength and axial load.

No.	Compressive strength (F_{cu}) (MPa)	Conventional columns	
		P_{FEM} (kN)	Stress in steel (MPa)
CSS1	20	542.00	194.67
CSS2	30	701.00	226.91
CSS3	40	880.00	263.17
CSS4	50	1050.00	288.16
CSS5	60	1212.00	333.95
CSS6	70	1382.00	392.95
CSS7	80	1530.00	428.55
CSS8	90	1721.00	473.61
CSS9	100	1921.00	525.33

Table 7: Effect of stress in steel bars at the different compressive strength of concrete.

Effect of reinforcement ratio

To study the influence of the longitudinal reinforcement ratio (ϱ) on the behavior of conventional RC columns and RC composite columns, analyses were performed for four different values: 0.79%, 1.23%, 1.77%, and 3.14% using reinforcement diameters of 8 mm, 10 mm, 12 mm, and 16 mm, respectively. The analysis was conducted with a concrete compressive strength of 40 MPa and steel yield strength of 400 MPa.

The theoretical calculated maximum axial loads and the numerical maximum axial loads are presented in Tab. 6 and Fig. 14. It is noted that the calculated maximum axial loads closely match the numerical values, with deviations not exceeding 4.48% for RC composite columns. Additionally, the theoretical calculated maximum axial loads increase when the reinforcement ratio is less than 1.25% and decrease when the reinforcement ratio exceeds 2.00%. Therefore, it may be necessary to reconsider the calculation of the value of axial load contribution resulting from the compressive stress in the reinforcing steel.

No.	RFT. Ratio (%)	Conventional columns			Composite columns		
		P_{Equ} (kN)	P_{FEM} (kN)	P_{FEM}/P_{Equ}	P_{Equ} (kN)	P_{FEM} (kN)	P_{FEM}/P_{PEqu}
RS1	0.79	761.15	821.00	1.08	1015.53	1061.00	1.04
RS2	1.23	803.37	842.00	1.05	1057.76	1100.00	1.04
RS3	1.77	854.98	860.00	1.01	1109.36	1121.00	1.01
RS4	3.14	986.35	891.00	0.90	1240.73	1220.00	0.98

Table 8: Effect of reinforcement ratio on theoretical and numerical maximum axial load.

Fig. 15 shows the relationship between the reinforcement ratio and axial load for both conventional RC columns and RC composite columns. It can be seen that the numerically maximum axial load increases linearly with the reinforcement ratio up to approximately 3% and then decreases for conventional RC columns. In contrast, the rate of increase remains linear for RC composite columns.

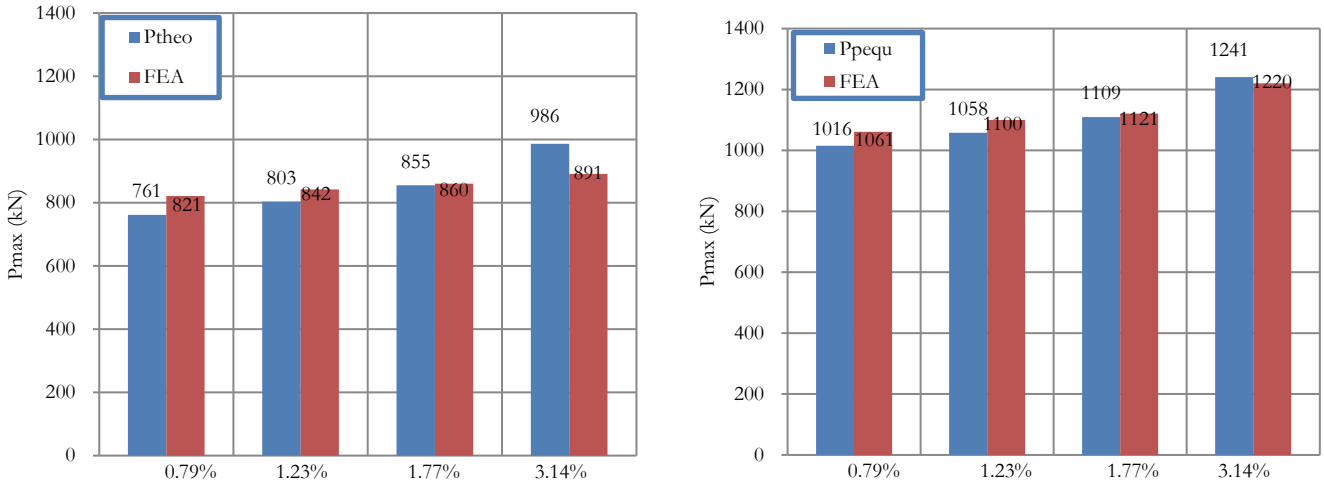

a) Conventional column b) Composite columns

Figure 14: Effect of the reinforcement ratio on theoretical and numerical maximum axial load.

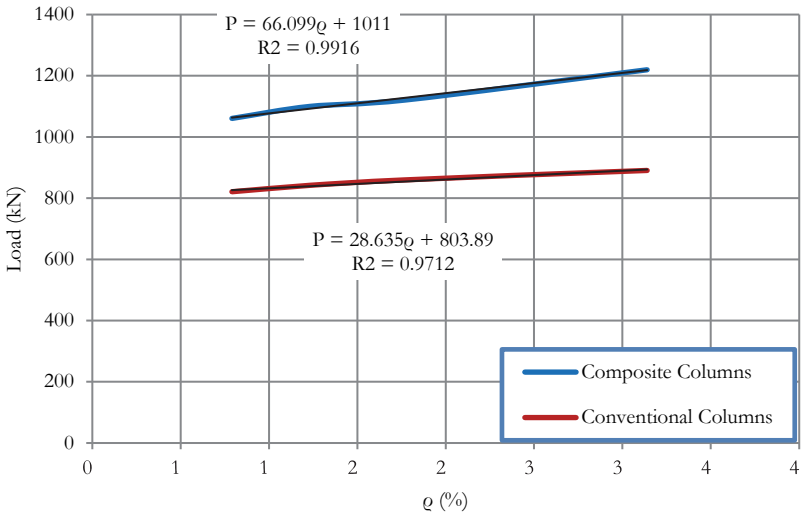

Figure 15: Relationship between reinforcement ratio and axial load.

No.	GFRP section	GFRP dimensions (mm)	GFRP I-section ratio (%)	P_{Equ} (kN)	P_{FEM} (kN)	P_{FEM} / P_{PEqu}	Stress in steel (Mpa)	Stress in GFRP (MPa)
RGFRP-P1	Flat Plate	89x5.5	2.03	899.91	935.00	1.04	349.05	181.41
RGFRP-P2		84x8	2.88	940.08	998.75	1.06	400.00	212.00
RGFRP-P3		80x10	3.52	970.55	1040.00	1.07	400.00	213.09
RGFRP-P4		76x12	4.13	999.52	995.00	1.00	362.04	166.67
RGFRP-P5		70x15	4.98	1040.20	980.00	0.94	359.82	140.53
RGFRP-P6		60x20	6.25	1058.35	980.00	0.93	301.61	116.70
RGFRP-I1	I-section	100x80x5.5	5.35	1057.76	1100.00	1.04	400.00	292.43
RGFRP-I2		100x80x8	7.63	1165.96	1107.50	0.95	400.00	199.97
RGFRP-I3		100x80x10	9.38	1249.17	1178.75	0.94	400.00	321.55
RGFRP-I4		100x80x12	11.06	1329.42	1195.00	0.90	400.00	205.90
RGFRP-I5		100x80x15	13.48	1444.21	1197.50	0.83	400.00	257.64
RGFRP-I6		100x80x20	17.18	1578.45	1210	0.77	338.93	147.14

Table 9: Effect of GFRP ratio on theoretical and numerical maximum axial load.

Effect of GFRP ratio

To investigate the influence of the GFRP ratio on the behavior of RC composite columns, analyses were performed for twelve different values ranging from 2.03% to 17.18% using two different shapes of GFRP sections, flat plates and I-shaped sections. The concrete compressive strength was set at 40 MPa and steel yield strength was 400 MPa.

The theoretically calculated maximum axial loads and the numerically maximum axial loads are presented in Tab. 7 and Fig. 16.

It can be seen that the calculated maximum axial loads closely match the numerical values for RC composite columns with GFRP ratio up to 4% for flat plates and 8% I-shaped sections. However, the numerically maximum axial loads remain almost constant at GFRP ratios exceeding 4% for flat plates and 8% I-shaped sections. Therefore, the proposed equation for calculating of the axial load of RC composite columns is satisfactory at GFRP ratios less than 4% for flat plates and 8% I-shaped sections.

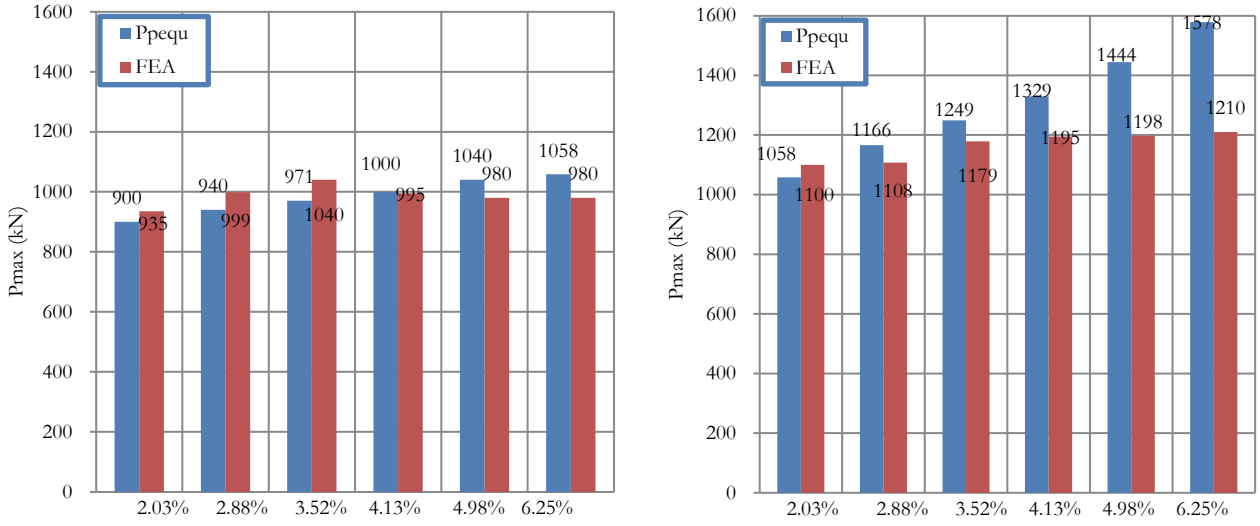

a) Flat Plate shape

b) I-Shape

Figure 16: Effect of the GFRP ratio on the theoretical and numerical maximum axial load.

The resistance of the RC composite columns is increases as the surface area of the GFRP increases and as the homogeneity inside within the concrete section improves.

CONCLUSIONS

From studying the proposed model for composite concrete columns consisting of Glass Fiber Reinforced Polymer (GFRP) profiles and longitudinal steel bars under axial compressive load, and from theoretical calculations for experimental tested columns specimens and theoretical columns by different codes, and from studying the behavior of axial compressive for composite concrete columns under different parameters factors, the following conclusions can be drawn:

- Glass Fiber Reinforced Polymer (GFRP) I-profile concrete composite columns have proven to be structurally efficient elements with high axial load capacity.
- Compared to the conventional RC columns, the RC composite columns with internal (GFRP) I-profile exhibited 17% higher ultimate capacity, and less displacement at the same loading levels.
- The axial load was reduced by approximately 14% and 39% for conventional RC column and RC composite column respectively when exposed to fire at temperature of 500 C° for one and half hours.
- The proposed theoretical equation accurately predicts the axial load of RC composite columns and should incorporate a reduction factor of 0.65 for the compressive strength of GFRP I-section.
- The numerical model predictions closely matched the experimental results. Across a wide range of load-bearing capacities the error between the finite element analysis and the experimental results was less than 1.5%.
- The Results indicated that the finite element model used in this study was able to predict the axial load of RC composite columns with reasonable accuracy.
- The numerical results indicated that the axial load capacity of the RC composite columns increased with a higher GFRP ratio, up to 4 % for flat plate and 8% for I-shaped profiles.
- The axial load increased with an increase in the compressive strength of concrete, longitudinal reinforcement ratio for both conventional RC columns and RC composite columns.
- The axial load did not increase proportionally with the increasing stress in the rebar, where the effective stress in the rebar did not exceed 300 MPa for concrete with compressive strength up to 50 MPa, and 525 MPa for high - strength concrete up to 100 MPa in conventional RC columns.

REFERENCES

[1] Hadi, M. and Youssef, J. (2016). Experimental investigation of GFRP-reinforced and GFRP-encased square concrete specimens under axial and eccentric load, and four-point bending test. Journal of Composites for Construction., 20(5). DOI: 10.1061/ (ASCE) CC.1943-5614.0000675.

[2] Jing, C., Zhao, L., Wu, T. and Li, W. (2024). Experimental and numerical simulation of reinforced concrete-filled square gfrp tubular columns under axial compression. Materials, 17 (11). DOI: 10.3390/ma171125952024, 2595.

[3] Hadi, M., Wang, W. and Sheikh, M. (2015). Axial compressive behavior of GFRP tube reinforced concrete columns. Construction and Building Materials, 81, pp. 198-207. DOI:10.1016/j.conbuildmat.2015.02.025.

[4] Ishaqian, M. and Keramti, A. (2020). Performance of CFRP confined pultruded gfrp-concrete composite columns subjected to cyclic and monotonic compressive loading. Scilit, Sci And Tech Universal Inc In Scientia Iranica, 27(4), pp. 1685-1698. DOI: 10.24200/sci.2020.21803

[5] Harvey, J. (1993). A reinforced plastic footbridge, Aberfeldy, UK, Structural Engineering International, 3 (4), pp. 229-232. DOI: 10.2749/101686693780607589.

[6] Zouheir, A., Hashem, and Robert, L. (2001). Short vs. Long column behavior of pultruted glass-fiber reinforced polymer composites. Construction and Building Materials, 15(8), pp. 369-378. DOI: 10.1016/S0950-0618(01)00018-6.

[7] Xie, L., Bai, Y., Qi, Y. and Wang, H. (2019). Pultruded GFRP square hollow columns with bolted sleeve joints under eccentric compression. Composites Part B: Engineering, 162, pp. 274-282. DOI: 10.1016/j.compositesb.2018.11.001.

[8] Srinath, T. (2020). Buckling and bonding behavior of glass fiber reinforced epoxy resin composite column, International Journal of Electrical Engineering and Technology, 11 (9), pp. 219-224. DOI: 10.34218/IJEET.11.9.2020.022.

[9] Haba, S., Allawi, A. and Hindi, R. (2024). Experimental investigation of composite circular encased GFRP I-section concrete columns under different load conditions. Engineering, Technology & Applied Science Research, 14 (5), pp. 17286-17293. DOI: 10.48084/etasr.8521.

[10] Aydin, F. (2016). Effects of various temperatures on the mechanical strength of GFRP box profiles. Construction and Building Materials, 127, pp. 843-849. DOI: /10.1016/j.conbuildmat.2016.09.130.

[11] OPCT. Fiberglass Products Company, 398 Kaiyuan Road, Jizhou District, Hengshui City, Hebei Province, China, www.Chopct.com.

[12] Hassooni, A. and Zaidee, S. (2022). Behavior and strength of composite columns under the impact of uniaxial compression loading. Engineering Technology and Applied Science Research, 12(4), pp. 8843-8849. DOI: 10.48084/etasr.4753.

[13] Egyptian code for design and construction of reinforced concrete structures. (2020). Housing and Building National Research Center. Ministry of Housing, Utilities and Urban Planning, Giza, Egypt, ECP 203-2020.

[14] British Standards Institution. Structural use of concrete. (1997). Part 1: code of practice for design and construction. British Standards Institution, London, BS811O - 1997.

[15] ACI Committee. American Concrete. (2011). Institute, & International Organization for Standardization, Building code requirements for structural concrete and commentary. American Concrete Institute (ACI 318-11).

[16] European Standard. Design of concrete structures. (2011). part 1-1: General rules and rules for buildings. CEN, Brüssel, EN 1992-1-1, 2011.

[17] CSA Code Canadian Standards Association for Design of Concrete Structures. (2004). Consolidated Mailing, Canada CSA. A23.3-04, 2004.

[18] ANSYS. (2012). ANSYS Help, Release 19.

[19] MacGregor, G. (1992). Reinforced Concrete Mechanics and Design, Prentice-Hall, Inc., Englewood Cliffs, NJ, 1992.

NOTATION

A_{ft} Total cross-sectional area of GFRP I-section
Ag Gross area of the concrete column
A_{st} Total area of longitudinal reinforcement
E_s Modulus of elasticity of steel
f Stress at any strain ε
f_c' Ultimate cylinder compressive strength for concrete
f_{cu} Compressive strength of concrete
f_s Stress in steel bars when the concrete reaches the maximum strength

f_f Ultimate compressive strength of GFRP I-section
f_y The yield strength of steel
P_n Axial load at the maximum
a Ratio of average stress in rectangular compression block to the specified concrete strength
ε_c Strain in the concrete at reaching the maximum strength
η Reduction factor for the high strength concrete for the rectangular stress distribution
ϕ_c Resistance factor for concrete and equal to 1.0 for laboratory conditions
ϕ_s Resistance factor for steel and equal to 1.0 for laboratory conditions
ε_o Strain at the ultimate cylinder compressive strength f_c'